Photocatalytic Evaluation of Ag$_2$CO$_3$ for Ethylparaben Degradation in Different Water Matrices

Athanasia Petala [1][ORCID]**, Athanasia Nasiou [1], Dionissios Mantzavinos [1]**[ORCID]
and Zacharias Frontistis [2,*][ORCID]

[1] Department of Chemical Engineering, University of Patras, Caratheodory 1, University Campus, GR-26504 Patras, Greece; natpetala@chemeng.upatras.gr (A.P.); nancynasiou@gmail.com (A.N.); mantzavinos@chemeng.upatras.gr (D.M.)

[2] Department of Chemical Engineering, University of Western Macedonia, GR-50132 Kozani, Greece

[*] Correspondence: zfrontistis@uowm.gr

Abstract: The present study examines the photocatalytic properties of silver carbonate (Ag$_2$CO$_3$) for ethyl paraben (EP) degradation under simulated solar irradiation. Ag$_2$CO$_3$ was prepared according to a solution method and its physicochemical characteristics were studied by means of X-ray diffraction (XRD), the Brunauer–Emmett–Teller (BET) method, diffuse reflectance spectroscopy (DRS), and transmission electron microscopy (TEM). Complete EP (0.5 mg/L) removal was achieved after 120 min of irradiation with the use of 750 mg/L Ag$_2$CO$_3$ in ultrapure water (UPW), with EP degradation following pseudo-first-order kinetics. The effect of several experimental parameters was investigated; increasing catalyst concentration from 250 mg/L to 1000 mg/L led to an increase in EP removal, while increasing EP concentration from 0.25 mg/L to 1.00 mg/L slightly lowered k$_{app}$ from 0.115 min^{-1} to 0.085 min^{-1}. Experiments carried out with the use of UV or visible cut-off filters showed sufficient EP degradation under visible irradiation. A series of experiments were performed in real water matrices such as bottled water (BW) and wastewater (WW), manifesting Ag$_2$CO$_3$'s equally high photocatalytic activity for EP degradation. To interpret these results different concentrations of inorganic anions (bicarbonate 100–500 mg/L, chloride 100–500 mg/L) present in aqueous media, as well as 10 mg/L organic matter in the form of humic acid (HA), were added sequentially in UPW. Results showed accelerating effects on EP degradation for the lowest concentrations tested in all cases.

Keywords: advanced oxidation; endocrine disrupting compounds; waters; visible-light active materials

1. Introduction

A walk through the supermarket or pharmacy is enough to observe the phrase "paraben free" that appears today in some self-care mass market products. Parabens are p-hydroxybenzoates containing alkyl-side chains linked to an ester group that constitute a large group of preservatives capable of prolonging shelf life in many health and beauty products. Common parabens used are methylparaben, ethylparaben, butylparaben, and propylparaben. Their popularity is attributed to the fact that they possess a great number of desirable characteristics, such as broad antimicrobial spectrum, high efficiency, and low cost [1]. However, in recent years, many studies have pointed out the potential of these substances to act as endocrine disruptors or even carcinogens [2].

People are exposed to parabens through skin absorption or swallowing and then are excreted by urination. This, together with industrial activity, results in the entrance of parabens into the water cycle, leading to an indirectly continuous exposure of humans to parabens [3]. Despite the fact that removal efficiencies of parabens in wastewater treatment plants exceed 90%, they have still been detected in river water samples at low concentrations of the ng/L range [4], thus multiplying the

adverse effects both at humans and to the environment. The threat becomes bigger as parabens can react with bromides or chlorides present in waters, resulting in the generation of chlorinated and brominated species of high toxicity [5].

In order to address this issue, development of more effective technologies for decontamination of water and wastewater is of vital importance. Among many research efforts, advanced oxidation processes (AOPs) have come up with encouraging efficiencies [6–8].

Amongst AOPs, the photocatalytic approach seems to be the least energy-consuming and friendly to the environment. Of course, photocatalysis is not new, as it dates back to 1972, when Fujishima and Honda set up their photoelectrochemical cell [9]. However, the holy grail in recent years is the development of visible light active materials and their configuration under realistic conditions.

Up-to-date publications focusing on visible light active materials have pointed out bismuth vanadate ($BiVO_4$), graphitic carbon nitride (g-C_3N_4), and silver phosphate (Ag_3PO_4) as candidate photocatalytic materials with high efficiencies for degradation of recalcitrant micropollutants [10,11].

Apart from Ag_3PO_4, other silver-based materials hold a prominent position in the list of candidate photocatalytic materials, such as silver vanadate (Ag_3VO_4) [12], silver oxide (Ag_2O) [13], and silver halides (AgX, X:Cl, Br, I) [14]. In addition, Ag_2CO_3 has recently been reported to possess high activity toward the photocatalytic degradation of dyes such as methylene blue and rhodamine B [15]. Its satisfying photocatalytic performance is derived from the fact that the bottom of the conduction band (CB) in Ag_2CO_3 consists mainly of hybridized Ag s-Ag s states responsible for its high dispersity, which allows high photogenerated electrons mobility and prevents photogenerated charge carrier's recombination [15]. In order to increase its photocatalytic properties, a wide range of heterojunctions have also been synthesized, such as Ag_2CO_3/TiO_2 [16], $ZnO/Ag_2CO_3/Ag_2O$ [17], MoS_2/Ag_2CO_3 [18], and ZnO/Ag_2CO_3 [19].

However, most of these studies focus on optimizing the physicochemical and optical properties of Ag_2CO_3-based photocatalysts and tests are limited to dyes degradation, where there is always the possibility of photo-sensitization of the catalyst. Thus, the generalization of these results to other organic pollutants should be performed with caution [20]. Unlike this, the present study concentrates on Ag_2CO_3 photocatalytic activity in real and synthetic water matrices of environmental concern. The degradation of ethylparaben, a characteristic EDC agent, is studied under simulated solar light irradiation. In addition, several experimental parameters, such as catalyst concentration and ethylparaben initial concentration, are discussed in detail.

2. Materials and Methods

2.1. Materials and Water Matrices

Silver nitrate (($AgNO_3$, CAS: 7761-88-8) and sodium bicarbonate ($NaHCO_3$, CAS: 144-55-8) were purchased from Sigma-Aldrich and used for catalyst preparation as received, without further purification. Ethylparaben (EP) (HO-C_6H_4-CO-O-CH_2CH_3, CAS: 120-47-8), humic acid (HA, CAS: 1415-93-6), sodium chloride (NaCl, CAS: 7647-14-5), sodium bicarbonate ($NaHCO_3$, CAS: 144-55-8), and acetonitrile (CH_3CN, CAS: 75-05-8, for HPLC analysis) were also obtained from Sigma-Aldrich.

The main characteristics of water matrices used in the present study are (i) ultrapure water (UPW: 0.059 μS/cm conductivity, pH = 6.0), (ii) commercial bottled water (BW: 300 mg/L bicarbonate, 15 mg/L chloride, 5 mg/L nitrate, 12 mg/L sulphate, 387 μS/cm conductivity, pH = 7.4), and (iii) secondary treated wastewater (WW: pH = 8, conductivity = 0.38 mg/L, total organic carbon = 9 mg/L, total suspended solids = 2 mg/L, chemical oxygen demand = 26 mg/L).

2.2. Photocatalyst Preparation

Silver carbonate was prepared according to a simple solution method [21]. Half a gram of $NaHCO_3$ was added to 60 mL UPW (D1) under continuous stirring, while 2.04 g $AgNO_3$ were added in 60 mL UPW forming solution D2. D2 solution was then added dropwise in D1 solution and remained under

stirring at room temperature for 240 min. The precipitate was collected by centrifugation, washed with UPW and dried at 60 °C for 12 h.

2.3. Photocatalyst Characterization

The crystallographic structure of Ag_2CO_3 was investigated by means of X-ray diffraction (XRD) using an A Brucker D8 Advance instrument (Bruker, Karlsruhe, Germany) with a Cu Kα source (λ = 1.5496 Å). Data were collected in the 2θ range of 10° to 80° at a scan rate of 0.05° s^{-1} and a step size of 0.015°. Phase identification was based on JCPDS cards. Primary crystallite size was determined with the use of Debye–Scherrer's equation:

$$d = \frac{0.9\lambda}{B\cos\theta} \tag{1}$$

where B is the line broadening (in radians) at half of its maximum, θ is the diffraction angle and λ is the X-ray wavelength corresponding to Cu Ka radiation (0.15406 nm). Specific surface area was determined according to the Brunauer–Emmett–Teller (BET) method with the use of a Micromeritics (Gemini III 2375) instrument (Norcross, GA, USA). For the determination of optical properties, diffuse reflectance spectroscopy (DRS, Varian Cary 3, Agilent 5301 Stevens Creek Blvd, Santa Clara, CA 95051, USA) was adopted. Spectrophotometer was equipped with an integration sphere, using $BaSO_4$ as a reference. Photocatalysts were loaded into a quartz cell, and spectra were obtained in the wavelength range of 200–800 nm. Transmission electron microscopy (TEM) images were recorded using a JEOL JEM-2100 system (JEOL, Akishima, Tokyo, Japan) operated at 200 kV (resolution: point 0.23 nm, lattice 0.14 nm). Films (Kodak SO-163) were used for recording HR-TEM images. The specimens were prepared by dispersion in water and spread onto a carbon-coated copper grid (200 mesh).

2.4. Photocatalytic Experiments

A typical photocatalytic degradation experiment can be described as follows: A measured volume of a stock EP solution (10 mg/L) is added to 120 mL of the water matrix (usually UPW) in order to achieve the desired initial EP concentration (0.5 mg/L in most cases). A pre-weighted amount of photocatalyst is then added to the solution (typically 750 mg/L). The photoreactor (a glass cylindrical vessel) is stirred at 400 rpm for 15 min in the dark to achieve complete adsorption/desorption equilibrium of EP on the photocatalyst surface. After this period, the suspension is irradiated employing a solar simulator (Oriel, model LCS-100, Newport, Irvine, CA, USA) equipped with a 100 W xenon ozone-free lamp) at an incident intensity of 1.3×10^{-4} einstein/(m^2·s)., as measured by means of chemical actinometry [22]. Simulated solar radiation contains about 5% UVA radiation, and 0.1% UVB radiation. A 420 nm cut-off filter (Newport FSQ-GG420, 50.8 mm × 50.8 mm, Newport, Irvine, CA, USA) was employed for experiments performed under visible light. For experiments performed under visible light, the intensity was measured at 7×10^{-5} einstein/(m^2·s).

Most experiments were performed at matrix's inherent pH (pH = 6) except those where the initial pH was adjusted to acidic or alkaline conditions.

At regular time intervals, 1.2 mL volume samples are taken, filtered through a 0.2 μm PVDF filter and analyzed using high performance liquid chromatography (HPLC). Separation was achieved on a Kinetex XB-C18 100A column (Phenomenex, Torrance, CA, USA) (2.6 mm, 2.1 mm, 50 mm) and a 0.5 mm inline filter (Phenomenex, Torrance, CA, USA) (KrudKatcher Ultra) both purchased from Phenomenex. The mobile phase consisting of 75:25 water:acetonitrile eluted isocratically at 0.35 mL/min and 45 °C, while the injection volume was 40 mL. Detection was achieved through a photodiode array detector (Waters, Milford, MA, USA) (Waters 2996 PDA detector, detection l ¼ 254 nm). Details about HPLC measurements can be found elsewhere [23].

Most of the experiments were run in duplicate, and mean values are quoted as results, whose deviation never exceeded 5% in the range of concentrations tested.

3. Results

3.1. Characterization

The X-ray diffraction pattern of the as prepared Ag_2CO_3 is presented in Figure 1A. It is observed that all diffraction patterns can be indexed to the monoclinic phase of Ag_2CO_3 (JCPDS 12-766) without impurities. Characteristic peaks are indicated in Figure 1. The sharpness of the peaks indicates the high crystallinity of the sample, while the primary crystallite size is 44 nm (based on Equation (1)). Specific surface area according to BET method is lower than 1 m^2/g.
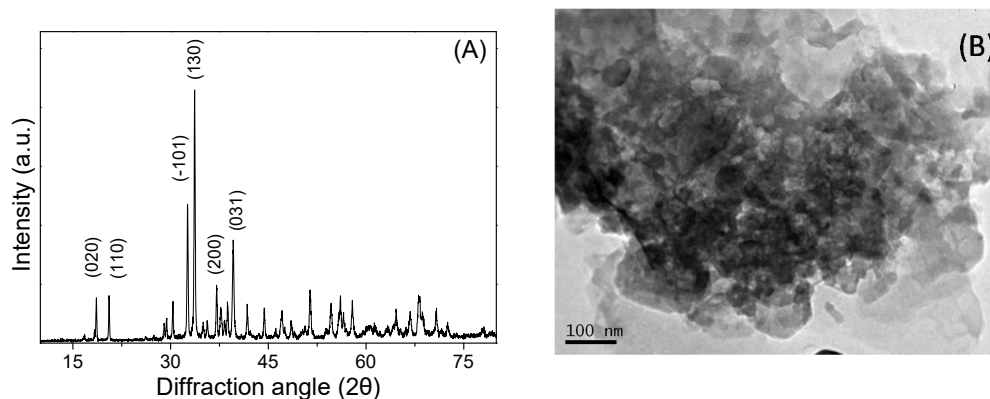

Figure 1. (**A**) X-ray diffraction (XRD) pattern and (**B**) transmission electron microscopy (TEM) image of Ag_2CO_3.

The optical properties of Ag_2CO_3 were studied with the use of (UV-vis) diffuse reflectance spectroscopy and the corresponding spectrum is shown in Figure 2. It is observed that Ag_2CO_3 has an absorption threshold at ~467 nm that allows to absorb a significant portion of visible light. Energy band gap was determined according to Tauc method and found equal to 2.6 eV (inset of Figure 2). Further information about the morphology of Ag_2CO_3 was collected from the TEM image (Figure 1B). It is observed that crystal size varies from 100–40 nm and is of almost spherical shape. Characterization results are in accordance with the literature for pure Ag_2CO_3 [16,21].
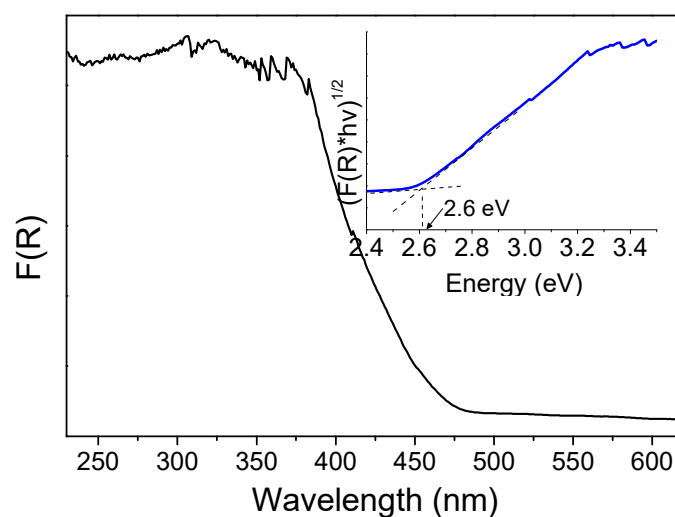

Figure 2. UV-vis diffuse reflectance spectra of Ag_2CO_3. Inset: Tauc plot of Ag_2CO_3.

3.2. Photocatalytic Activity of Ag_2CO_3

Figure 3 presents the photocatalytic performance at different concentrations of Ag_2CO_3 for 0.5 mg/L EP degradation in UPW under simulated solar irradiation. It is observed that, in the absence

of photocatalyst, practically no EP degradation takes place due to photolytic phenomena. The addition of only 250 mg/L Ag_2CO_3 results in almost 50% removal after 30 min, proving its high photocatalytic activity. Considering that EP degradation follows pseudo-first-order kinetics, the reaction rate can be expressed as follows [24]:

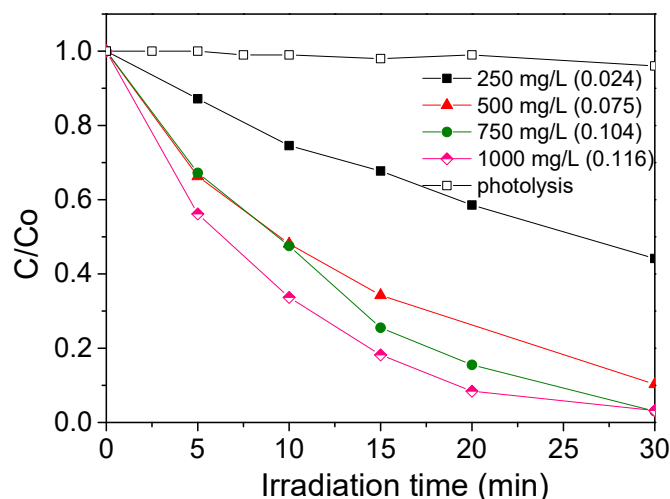$$\text{rate} = -\frac{d[\text{EP}]}{dt} = k_{app}[EP] \tag{2}$$

Figure 3. Effect of photocatalyst concentration on 0.5 mg/L EP degradation in ultrapure water (UPW). Numbers in brackets show apparent rate constants in min^{-1}.

Apparent rate constants (k_{app}) were calculated from the linearized form of Equation (2) and are shown in brackets. Doubling photocatalyst dosage from 250 mg/L to 500 mg/L accelerates EP degradation, resulting in 90% EP removal in the same time period. Further increase in Ag_2CO_3 concentration to 750 mg/L leads to an increase in k_{app} from 0.075 min^{-1} to 0.104 min^{-1}. In contrast, raising Ag_2CO_3 concentration to 1000 mg/L only slightly favors EP degradation, increasing k_{app} to 0.116 min^{-1}. The optimum photocatalyst dosage constitutes a special feature of each photocatalytic system highly connected not only to the activity of the photocatalytic material but also to the light penetration into the solution. As a result, the optimum value varies widely depending on the geometry and operating conditions of the photoreactor.

It is common knowledge that photocatalytic degradation of organic substances proceeds not only by direct reaction with photogenerated holes (h^+) but also indirectly through the formation of hydroxyl radicals ($^\bullet OH$). A prerequisite for $^\bullet OH$ formation is the valence band (VB) oxidation potential of the semiconductor to be located below the potential of $^\bullet OH$ formation (2.38 V vs NHE, pH = 7). In the case of Ag_2CO_3, VB is at 2.78 V vs NHE, pH = 7 [25], suggesting the participation of $^\bullet OH$ in EP degradation. Since the reaction takes place in the presence of oxygen, photogenerated electrons can also react with adsorbed O_2 resulting in the formation of additional oxidative species (mainly superoxide radical ($O_2^{\bullet-}$). Since optimization was not the goal of this work, a catalyst loading of 750 mg/L was selected for the continuation of this study.

Figure 4 shows the results obtained varying EP concentration in the range 0.25–1.00 mg/L. It is observed that a k_{app} equal to 0.115 min^{-1} is obtained for the lower EP concentration tested. Increasing EP concentration to 1.00 mg/L resulted in only a slight decrease in k_{app} to 0.085 min^{-1}.

Comparable irradiation times have been reported in case of organic dyes degradation under visible light irradiation with the use of Ag_2CO_3; H. Dong et al [15] showed that 10 mg/L methyl orange and 10 mg/L rhodamine B was removed from ultrapure water in 15 min and 35 min, respectively, with 0.5 g/L Ag_2CO_3. Moreover, the as prepared Ag_2CO_3 photocatalyst has similar activity with heterostructures that include it. Specifically, Ag_2CO_3/ZnO led to complete rhodamine B degradation

after 120 min of visible light irradiation [19], while Ag_2CO_3/MoS_2 composite photocatalysts degraded Lanasol Red 5B in 25 min [18]. However, these works study photocatalytic degradation of dyes and not micropollutants, in which the results are often overrated due to photo-sensitization of the catalyst.
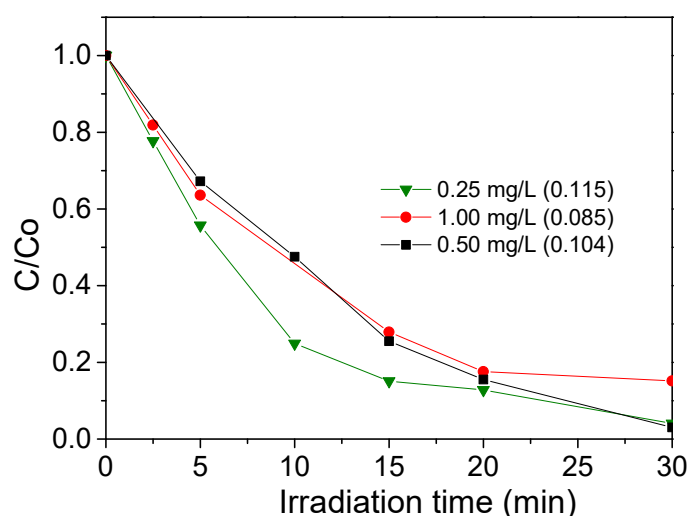

Figure 4. Effect of EP concentration on its photocatalytic degradation with 750 mg/L Ag_2CO_3 in UPW. Numbers in brackets show apparent rate constants in min^{-1}.

3.3. Effect of Type of Irradiation

Diffuse reflectance spectroscopy showed that Ag_2CO_3 can absorb a significant portion of light in the visible region (Figure 2). To confirm this, additional experiments were carried out under visible or UV light with the use of appropriate cut-off filters. As seen in Figure 5, an almost 55% removal is achieved after 20 min under visible light alone and this increases to 75% under UV light, thus implying that the photocatalyst is responsive in the visible part of the spectrum.
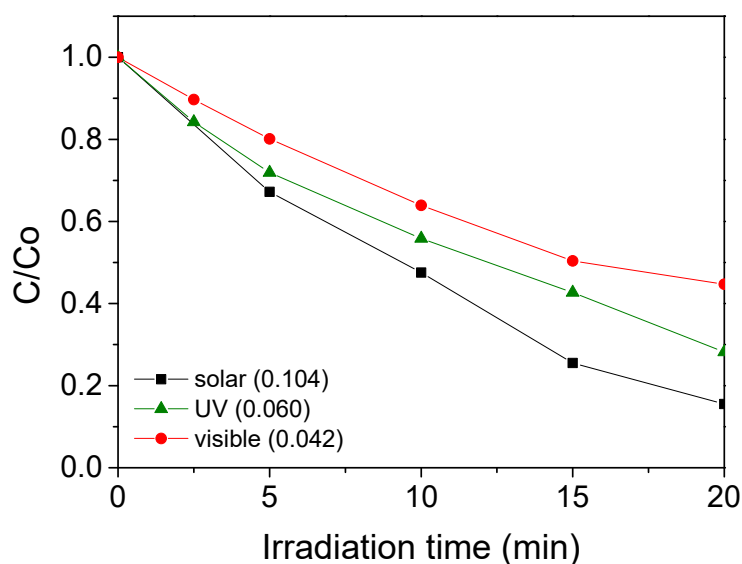

Figure 5. Effect of type of irradiation on 0.5 mg/L EP degradation with 750 mg/L Ag_2CO_3 in UPW. Numbers in brackets show apparent rate constants in min^{-1}.

3.4. Effect of the Water Matrix

In order to test the present photocatalytic system under more realistic conditions, a new set of experiments were conducted in real water matrices, such as BW and WW. Both organic and inorganic

components present in aqueous media could modify the route of micropollutants photocatalytic degradation pathways, thus either accelerating or slowing down the overall performance [26]. In most cases, hindering effects become more significant as the water matrix complexity increases. However, this cannot be considered as a rule, as highly promoting effects have also been reported in complex aqueous media.

Figure 6 presents the degradation of 0.5 mg/L EP with 750 mg/L Ag_2CO_3 in UPW, BW, and WW. Noticeably, there is only a minor decrease in k_{app} from 0.104 in UPW to 0.080 min^{-1} in BW and WW. In order to interpret these results, further experiments were performed in UPW spiked with (i) humic acid (HA), an analogue of the natural organic matter found in waters/wastewaters, and (ii) bicarbonate and chloride as the most common inorganic anions.
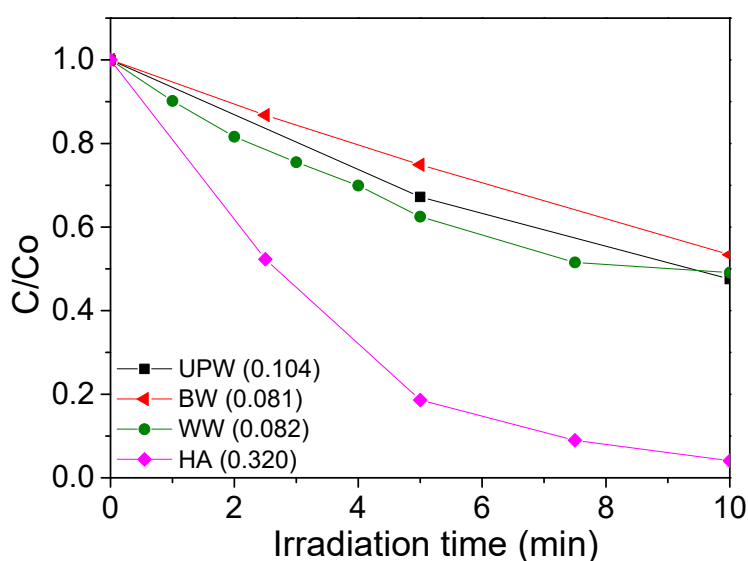

Figure 6. Effect of water matrix (BW, WW) and 10 mg/L HA on 0.5 mg/L EP degradation with 750 mg/L Ag_2CO_3. Numbers in brackets show apparent rate constants in min^{-1}.

The effect of 10 mg/L HA on EP degradation is also shown in Figure 6. It is observed that EP removal was greatly enhanced, with k_{app} increasing to 0.320 min^{-1}. This may be attributed to the fact that (i) organic compounds naturally occurring in effluents can act as photosensitizers of the photocatalyst (through electron transfer from HA to semiconductor) [27] and/or (ii) electron transfer from photocatalyst conduction band to HA may occur, thus suppressing electron-hole recombination and, consequently, enhancing photodegradation rates [28]. Other enhancing effects may include (iii) the photosensitization activity of organic species that can promote the production of reactive oxygen species (ROS) by UV irradiation, resulting in indirect photolysis of micropollutants [29], and (iv) the homolysis of organic matter producing additional reactive radicals able to oxidize micropollutants either directly or indirectly through reaction with oxygen and formation of additional ROS [30].

The effect of bicarbonate on EP degradation with the use of 750 mg/L Ag_2CO_3 is presented in Figure 7A. Addition of 100 mg/L bicarbonate increases significantly EP removal with kapp increasing from 0.104 to 0.578 min^{-1}. A further increase to 250 mg/L or 500 mg/L lowers EP degradation rate, which is, however, greater than in UPW. This contradicts the majority of previous studies that usually report retardation effects associated with the scavenging of hydroxyl radicals by bicarbonate and the formation of carbonate radicals ($HCO_3^{\bullet}$) with lower oxidation potential [31]. In a previous work, we found that the presence of bicarbonate quenched the recombination of photogenerated carriers and this led an increased production of $^{\bullet}OH$ [32]. Moreover, ($HCO_3^{\bullet}$) is a one-electron oxidant that acts by both electron transfer and hydrogen abstraction mechanisms producing ROS from the oxidized compounds, which could partly counteract the scavenging of $^{\bullet}OH$ [33].
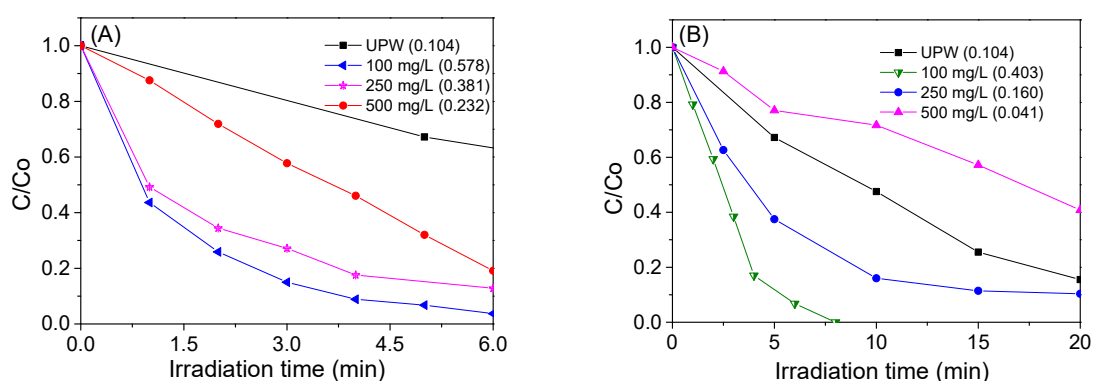
Figure 7. Effect of (**A**) bicarbonate and (**B**) chloride on 0.5 mg/L EP degradation with 750 mg/L Ag_2CO_3. Numbers in brackets show apparent rate constants in min^{-1}.

The effect of chloride on EP degradation is depicted in Figure 7B. Addition of 100 mg/L chloride leads to complete EP removal in less than 8 min, which is almost three times faster than in UPW. Increasing chloride concentration to 250 mg/L hampers EP removal, decreasing k_{app} from 0.403 to 0.160 min^{-1}, but this still is faster than in UPW. Only at 500 mg/L chloride, does EP degradation slow down considerably with the k_{app} becoming 0.041 min^{-1}. In general, addition of chloride (Cl^-) in UPW could lead to the following reactions:

$$HO^\bullet + Cl^- \rightarrow Cl^\bullet + HO^- \tag{3}$$

$$Cl^- + Cl^\bullet \rightarrow Cl_2^{\bullet -} \tag{4}$$

Moreover, several consecutive reactions may take place leading to the formation of additional chlorine-containing radicals such as $Cl^\bullet$, $Cl_2^{\bullet -}$, $ClOH^{\bullet -}$ [26,34]. While these reactions may be responsible for scavenging $^\bullet OH$ or blocking catalyst active sites, beneficial effects have also been reported in similar systems [35,36]; these may be related to the higher selectivity of chlorine radicals, thus altering degradation pathways.

Overall, major organic and inorganic, non-target constituents inherently found in waters seem not to inhibit the photocatalytic performance of Ag_2CO_3 and this has been demonstrated in experiments with environmental samples, i.e., BW and WW. A synergistic but yet complex interplay amongst the matrix's organic and inorganic constituents, the photocatalyst and the substate under consideration may explain this observation.

3.5. Effect of pH

The effect of changing the initial pH in the range 3–9 on 0.5 mg/L EP degradation in UPW was also tested and the results are shown in Figure 8. It seems that a shift from inherent, near-neutral conditions (i.e., pH = 6) to an alkaline environment does not have a considerable effect on EP degradation, with k_{app} only slightly decreasing from 0.104 to 0.081 min^{-1}. This could be explained considering the matching or mismatching between the catalyst's surface charge and the organic molecule's ionization state. Indeed, the pKa value of EP is 8.34 [4], while Ag_2CO_3 has been reported to change surface charge under highly basic conditions [37]. These observations agree with M. Guo et al. [37] and E. Nyankson et al. [38] who studied the photocatalytic performance of $AgBr/Ag_2CO_3$ and Ag_2CO_3-halloysite nanotubes respectively, showing the dependence of photocatalytic activity on pH, with favoring effects taking place under neutral and basic conditions.

EP removal is significantly accelerated at acidic conditions. In general Ag-based semiconductors are unstable under acidic media [37], as shown in reuse experimental runs (Figure 9A,B). Dissolution of Ag_2CO_3 in acidic media to silver ions may trigger homogeneous photocatalytic phenomena, thus explaining the increased reactivity.
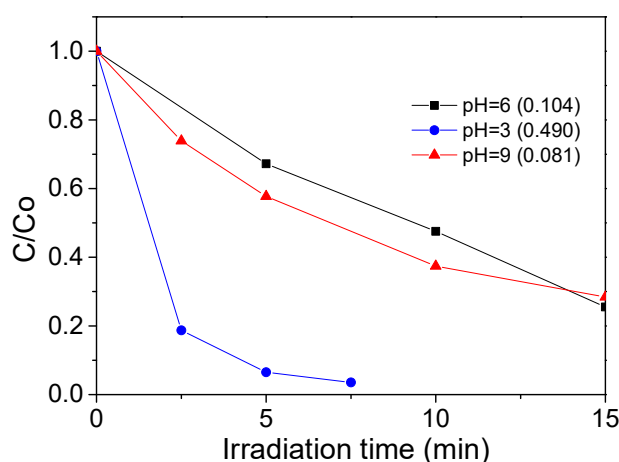
Figure 8. Effect of initial solution pH on 0.5 mg/L EP degradation with 750 mg/L Ag_2CO_3. Numbers in brackets show apparent rate constants in min^{-1}.
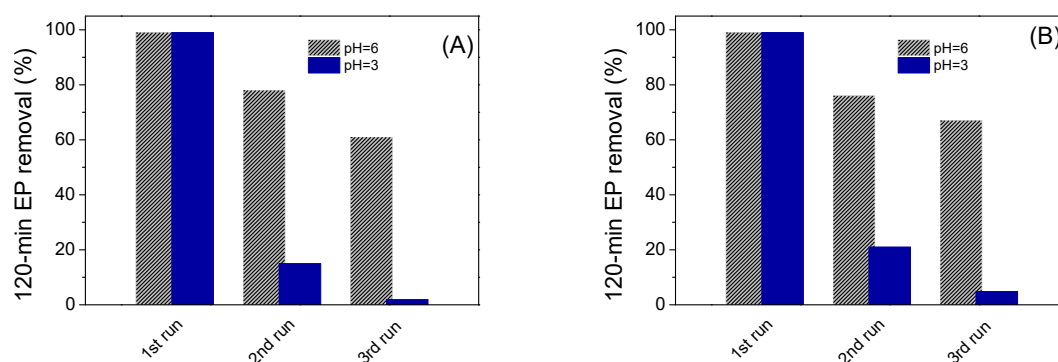

Figure 9. Change of photocatalytic activity of Ag_2CO_3 upon repeated use for the degradation of 0.5 mg/L EP in UPW in neutral and acidic pH under (**A**) solar irradiation and (**B**) UV irradiation.

This said, most environmental matrices have pH values between 6 and 8, i.e., a pH range where silver leaching is unlikely to occur to a considerable degree.

3.6. Catalyst Reuse

Reusability tests were carried out using 750 mg/L Ag_2CO_3 under neutral (pH = 6) and acidic conditions (pH = 3) in UPW using solar and UV light irradiation. To do so, 750 mg/L of fresh Ag_2CO_3 was added in 120 mL of ultrapure water containing 0.5 mg/L EP and the mixture was then subject to irradiation for 120 min; at the end of this period, EP conversion was monitored and the mixture was added the necessary amount of EP to bring its initial concentration back to 0.5 mg/L. This cycle was repeated twice, while no other conditioning took place. Figure 9A shows the performance of the recycled Ag_2CO_3 catalyst for EP degradation for three consecutive runs. It is observed that under neutral conditions EP removal reduces to ~80% after the first run. This is probably attribute to stability issues related with silver-based catalysts. This reduction is more pronounced in the third cycle were EP removal drops to 60%. On the other hand, under acidic conditions, it is observed that after the first run, EP removal drops practically to zero, implying complete dissolution of Ag_2CO_3 at this pH.

The same experimental runs were carried out with the use of the appropriate visible light cut off filter and results are presented in Figure 9B. It is observed that results are qualitatively the same under UV and solar irradiation, showing that stability issues of Ag_2CO_3 are probably related with the UV part of solar irradiation and not to the visible.

From these preliminary results, it is clear that future research should be directed to a systematic check of the stability of the Ag_2CO catalyst in a continuous flow reactor and to examine whether the

amount of silver ions exceeds the environmental limits. Also, technologies such as adsorption to biochar [39] can be used to recover silver, thus providing a complete solution in the context of the circular economy.

3.7. Comparison with Different Advanced Oxidation AOPs

The results presented in this work are in accordance with previous studies of our group investigating the photocatalytic degradation of EP with (i) $CuO_x/BiVO_4$ photocatalysts, yielding complete removal after 60 min [40], and (ii) ZnO suspensions leading to complete removal after 20 min [41]. These yields are of the same order of magnitude or even higher than the state of art TiO_2 (Degussa P25) photocatalyst, showing complete 1 mg/L EP removal in ~30 min [41]. It should be noted here that ZnO and TiO_2 are UV-light responsive materials with efficiencies under visible light be close to zero. In two recent studies, Fernandes et al [3] achieved complete EP removal after ~20 min using lab-made g-C_3N_4, while Guo et al [42] showed that $AgCl/Ag_3PO_4$ photocatalysts led to 98% EP removal (20 mg/L) in 40 min of solar irradiation. The superiority of the present system derives from the fact that it retains its activity in real water matrices, increasing its practical value. Moreover, Ag_2CO_3 showed practically the same activity under visible and UV irradiation, establishing itself as a true visible light active photocatalytic material. Information regarding EP photocatalytic degradation is collected in Table 1.

Table 1. EP photocatalytic degradation with different materials.

Photocatalyst	EP Concentration (mg/L)	Catalyst Concentration (mg/L)	Type of Irradiation	Time Period for Complete Degradation (min)	References
0.75(% wt.) $CuO_x/BiVO_4$	2	1000	solar	60	[40]
ZnO	1	250	solar	20	[41]
TiO_2(P25)	1	250	solar	30	[41]
g-C_3N_4	13	1000	visible	20	[3]
$AgCl/Ag_3PO_4$	20	500	visible	40	[42]
Ag_2CO_3	0.5	750	solar	30	[This work]

Apart from photocatalysis, EP removal has also been tested by other AOPs and characteristic examples are presented in Table 2. In the case of heat-activated persulfate (PS), complete EP removal (3 mg/L) was achieved after 240 min of reaction in UPW, but the reaction was impeded when the matrix was spiked with organic matter [43]. In addition, UVC-activated persulfate has been adopted for EP removal resulting in complete degradation in UPW in 90 min [44]. EP degradation (0.2 mg/L) has also been achieved by anodic oxidation over boron-doped diamond yielding complete removal within 20 min at 70 mA/cm^2 in 0.1 M Na_2SO_4 electrolyte [45].

Table 2. EP removal with different advanced oxidation processes (AOPs).

System	EP Concentration (mg/L)	Time Period for Complete Degradation (min)	Experimental Parameters	References
Heat-activated/PS	3	240	[EP]:20 mM, pH: 7, 60 °C [persulfate]:1mM.	[43]
UV-C/PS	5	90	[EP]:30 mM, [PS =PMS]:0.25-2.5 mM	[44]
Electrochemical oxidation	0.2	20	[EP]:200 mg/L in 0.1 M Na_2SO_4 i:70 mA/cm^2	[45]
Ag_2CO_3/solar irradiation	0.5	30	[catalyst]:750 mg/L, pH:6	[This work]

4. Conclusions

In this work, a visible light responsive Ag_2CO_3 photocatalyst was successfully prepared by a simple solution method. A series of experiments were carried out for ethylparaben degradation under simulated solar light irradiation. The main conclusions are as follows:

- Ag_2CO_3 shows substantial activity for EP degradation in UPW under both solar and visible light irradiation.
- The presence of ions such as bicarbonates and chlorides in concentrations found in environmental samples improves performance.
- Of particular interest is that the presence of humic acid significantly increases the degradation of EP.
- As a result, Ag_2CO_3 retains its activity in more complex, environmentally relevant matrices, like secondary treated wastewater and bottled water.
- Ag_2CO_3 photocatalytic properties are similar with other photocatalytic systems studying organic dyes degradation under visible light irradiation with the use of Ag_2CO_3. Moreover, its activity is of the same order of magnitude as very promising photocatalytic materials such as $CuO_x/BiVO_4$ and g-C_3N_4.
- In terms of efficiency, the proposed system appears to be competitive with other energy-intensive processes such as electrochemical oxidation and heat-activated persulfate and further research is needed in this direction.
- Future research should move towards exploring the stability of Ag_2CO_3, in a continuous flow configuration, as well as examining environmental and low-cost methods of silver recovery.

References

1. Bilal, M.; Iqbal, H.M.N. An insight into toxicity and human-health-related adverse consequences of cosmeceuticals—A review. *Sci. Total Environ.* **2019**, *670*, 555–568. [CrossRef]
2. Wang, Z.; Dinh, D.; Scott, W.C.; Williams, E.S.; Ciarlo, M.; DeLeo, P.; Brooks, B.W. Critical review and probabilistic health hazard assessment of cleaning product ingredients in all-purpose cleaners, dish care products, and laundry care products. *Environ. Int.* **2019**, *125*, 399–417. [CrossRef] [PubMed]
3. Fernandes, R.A.; Sampaio, M.J.; Dražić, G.; Faria, J.L.; Silva, C.G. Efficient removal of parabens from real water matrices by a metal-free carbon nitride photocatalyst. *Sci. Total Environ.* **2019**, *716*, 135346. [CrossRef] [PubMed]
4. Haman, C.; Dauchy, X.; Rosin, C.; Munoz, J.-F. Occurrence, fate and behavior of parabens in aquatic environments: A review. *Water Res.* **2015**, *68*, 1–11. [CrossRef] [PubMed]
5. Álvarez, M.A.; Ruidíaz-Martínez, M.; Cruz-Quesada, G.; López-Ramón, M.V.; Rivera-Utrilla, J.; Sánchez-Polo, J.M.; Mota, A.J. Removal of parabens from water by UV driven advanced oxidation processes. *Chem. Eng. J.* **2020**, *379*, 122334. [CrossRef]

6. Boczkaj, G.; Fernandes, A. Wastewater treatment by means of Advanced Oxidation Processes at basic pH conditions: A review. *Chem. Eng. J.* **2017**, *320*, 608–633. [CrossRef]

7. Dewil, R.; Mantzavinos, D.; Poulios, I.; Rodrigo, M.A. New perspectives for Advanced Oxidation Processes. *J. Environ. Manag.* **2017**, *195*, 93–99. [CrossRef]

8. Frontistis, Z. Degradation of the nonsteroidal anti-inflammatory drug piroxicam from environmental matrices with UV-activated persulfate. *J. Photochem. Photobiol. A Chem.* **2019**, *378*, 17–23. [CrossRef]

9. Fujishima, A.; Honda, K. Electrochemical Photolysis of Water at a Semiconductor Electrode. *Nature* **1972**, *238*, 37–38. [CrossRef]

10. Byrne, C.; Subramanian, G.; Pillai, S.C. Recent advances in photocatalysis for environmental applications. *J. Environ. Chem. Eng.* **2018**, *6*, 3531–3555. [CrossRef]

11. Yu, H.; Wang, D.; Zhao, B.; Lu, Y.; Wang, X.; Zhu, S.; Qin, W.; Huo, M. Enhanced photocatalytic degradation of tetracycline under visible light by using a ternary photocatalyst of $Ag_3PO_4/AgBr/g-C_3N_4$ with dual Z-scheme heterojunction. *Sep. Purif. Technol.* **2020**, *237*, 116365. [CrossRef]

12. Mei, F.; Dai, K.; Zhang, J.; Li, W.; Liang, C. Construction of Ag SPR-promoted step-scheme porous $g-C_3N_4/Ag_3VO_4$ heterojunction for improving photocatalytic activity. *Appl. Surf. Sci.* **2019**, *488*, 151–160. [CrossRef]

13. Tomara, T.; Frontistis, Z.; Petala, A.; Mantzavinos, D. Photocatalytic performance of Ag_2O towards sulfamethoxazole degradation in environmental samples. *J. Environ. Chem. Eng.* **2019**, *7*, 103177. [CrossRef]

14. Zou, X.J.; Dong, Y.Y.; Li, S.J.; Ke, J.; Cui, Y.B. Facile anion exchange to construct uniform AgX (X = Cl, Br, I)/Ag_2CrO_4 NR hybrids for efficient visible light driven photocatalytic activity. *Sol. Energy* **2018**, *169*, 392–400. [CrossRef]

15. Dong, H.; Chen, G.; Sun, J.; Li, C.; Yu, Y.; Chen, D. A novel high-efficiency visible-light sensitive Ag_2CO_3 photocatalyst with universal photodegradation performances: Simple synthesis, reaction mechanism and first-principles study. *Appl. Catal. B Environ.* **2013**, *134*, 46–54. [CrossRef]

16. Feng, C.; Li, G.; Ren, P.; Wang, Y.; Huang, X.; Li, D. Effect of photo-corrosion of Ag_2CO_3 on visible light photocatalytic activity of two kinds of Ag_2CO_3/TiO_2 prepared from different precursors. *Appl. Catal. B Environ.* **2014**, *158*, 224–232. [CrossRef]

17. Rosman, N.; Norharyati, W.; Salleh, W.; Fauzi Ismail, A.; Jaafar, J.; Harun, Z.; Aziz, F.; Azuwa Mohamed, M.; Ohtani, B.; Takashima, M. Photocatalytic degradation of phenol over visible light active $ZnO/Ag_2CO_3/Ag_2O$ nanocomposites heterojunction. *J. Photoch. Photobio. A* **2018**, *364*, 602–612. [CrossRef]

18. Fu, S.; Yuan, W.; Yan, Y.; Liu, H.; Shi, X.; Zhao, F.; Zhou, J. Highly efficient visible-light photoactivity of Z-scheme MoS_2/Ag_2CO_3 photocatalysts for organic pollutants degradation and bacterial inactivation. *J. Environ. Manag.* **2019**, *252*, 109654. [CrossRef]

19. Li, X.; Liu, D.; Zhu, B.; Wang, J.; Lang, J. Facile preparation of ZnO/Ag_2CO_3 heterostructured nanorod arrays with improved photocatalytic activity. *J. Phys. Chem. Solids* **2019**, *125*, 96–102. [CrossRef]

20. Rochkind, M.; Pasternak, S.; Paz, Y. Using Dyes for Evaluating Photocatalytic Properties: A Critical Review. *Molecules* **2015**, *20*, 88–110. [CrossRef]

21. Yu, C.; Li, G.; Kumar, S.; Yang, K.; Jin, R. Phase transformation synthesis of novel Ag_2O/Ag_2CO_3 heterostructures with high visible light efficiency in photocatalytic degradation of pollutants. *Adv. Mater.* **2014**, *26*, 892–898. [CrossRef] [PubMed]

22. Patsoura, A.; Kondarides, D.I.; Verykios, X.E. Enhancement of photoinduced hydrogen production from irradiated Pt/TiO_2 suspensions with simultaneous degradation of azo-dyes. *Appl. Catal. B Environ.* **2006**, *64*, 171–179. [CrossRef]

23. Petala, A.; Frontistis, Z.; Antonopoulou, M.; Konstantinou, I.; Kondarides, D.I.; Mantzavinos, D. Kinetics of ethyl paraben degradation by simulated solar radiation in the presence of N-doped TiO_2 catalysts. *Water Res.* **2015**, *81*, 157–166. [CrossRef] [PubMed]

24. Dimitrakopoulou, D.; Rethemiotaki, I.; Frontistis, Z.; Xekoukoulotakis, N.P.; Venieri, D.; Mantzavinos, D. Degradation, mineralization and antibiotic inactivation of amoxicillin by UV-A/TiO_2 photocatalysis. *J. Environ. Manag.* **2012**, *98*, 168–174. [CrossRef]

25. Rosman, N.; Norharyati, W.; Salleh, W.; Aziz, F.; Ismail, A.F.; Harun, Z.; Syamsol Bahri, S.; Nagai, K. Electrospun Nanofibers Embedding $ZnO/Ag_2CO_3/Ag_2O$ Heterojunction Photocatalyst with Enhanced Photocatalytic Activity. *Catalysts* **2019**, *9*, 565. [CrossRef]

26. Lado Ribeiro, A.R.; Moreira, N.F.F.; Li Puma, G.; Silva, A.M.T. Impact of water matrix on the removal of micropollutants by advanced oxidation technologies. *Chem. Eng. J.* **2019**, *363*, 155–173. [CrossRef]

27. Postigo, C.; Sirtori, C.; Oller, I.; Malato, S.; Maldonado, M.I.; López de Alda, M.; Barceló, D. Solar transformation and photocatalytic treatment of cocaine in water: Kinetics, characterization of major intermediate products and toxicity evaluation. *Appl. Catal. B Environ.* **2011**, *104*, 37–48. [CrossRef]

28. Cho, Y.; Choi, W. Visible light-induced reactions of humic acids on TiO_2. *J. Photochem. Photobiol. A Chem.* **2002**, *148*, 129–135. [CrossRef]

29. Beltrán, F.J.; Aguinaco, A.; García-Araya, J.F. Application of ozone involving advanced oxidation processes to remove some pharmaceutical compounds from urban wastewaters. *Ozone Sci. Eng.* **2012**, *34*, 3–15. [CrossRef]

30. Repousi, V.; Petala, A.; Frontistis, Z.; Antonopoulou, M.; Konstantinou, I.; Kondarides, D.I.; Mantzavinos, D. Photocatalytic degradation of bisphenol A over Rh/TiO_2 suspensions in different water matrices. *Catal. Today* **2017**, *284*, 59–66. [CrossRef]

31. Jallouli, N.; Pastrana-Martínez, L.M.; Ribeiro, A.R.; Moreira, N.F.F.; Faria, J.L.; Hentati, O.; Silva, A.M.T.; Ksibi, M. Heterogeneous photocatalytic degradation of ibuprofen in ultrapure water, municipal and pharmaceutical industry wastewaters using a TiO_2/UV-LED system. *Chem. Eng. J.* **2018**, *334*, 976–984. [CrossRef]

32. Kanigaridou, Y.; Petala, A.; Frontistis, Z.; Antonopoulou, M.; Solakidou, M.; Konstantinou, I.; Deligiannakis, Y.; Mantzavinos, D.; Kondarides, D.I. Solar photocatalytic degradation of bisphenol A with $CuO_x/BiVO_4$: Insights into the unexpectedly favorable effect of bicarbonates. *Chem. Eng. J.* **2017**, *318*, 39–49. [CrossRef]

33. Augusto, O.; Bonini, M.G.; Amanso, A.M.; Linares, E.; Santos, C.C.; Lopes de Menezes, S. Nitrogen dioxide and carbonate radical anion: Two emerging radicals in biology. *Free Radic. Biol. Med.* **2002**, *32*, 841–859. [CrossRef]

34. Rioja, N.; Zorita, S.; Penas, F.J. Effect of water matrix on photocatalytic degradation and general kinetic modeling. *Appl. Catal. B Environ.* **2016**, *180*, 330–335. [CrossRef]

35. Ioannidi, A.; Frontistis, Z.; Mantzavinos, D. Destruction of propyl paraben by persulfate activated with UV-A light emitting diodes. *J. Environ. Chem. Eng.* **2018**, *6*, 2992–2997. [CrossRef]

36. Outsiou, A.; Frontistis, Z.; Ribeiro, R.S.; Antonopoulou, M.; Konstantinou, I.K.; Silva, A.M.T.; Faria, J.L.; Gomes, H.T.; Mantzavinos, D. Activation of sodium persulfate by magnetic carbon xerogels (CX/CoFe) for the oxidation of bisphenol A: Process variables effects, matrix effects and reaction pathways. *Water Res.* **2017**, *124*, 97–107. [CrossRef] [PubMed]

37. Guo, M.; Wang, L.; Cai, Y.; Li, F.; Zhang, M.; Wang, J.; Zhao, D.; Shen, Y. Effect of pH value on photocatalytic performance and structure of $AgBr/Ag_2CO_3$ heterojunctions synthesized by an in situ growth method. *J. Electron. Mater.* **2020**, *49*, 3301–3308. [CrossRef]

38. Nyankson, E.; Agyei-Tuffour, B.; Annan, E.; Yaya, A.; Mensah, B.; Onwona-Agyeman, B.; Amedalor, R.; Kwaku-Frimpong, B.; Efavi, J.K. Ag_2CO_3-halloysite nanotubes composite with enhanced removal efficiency for water soluble dyes. *Heliyon* **2019**, *5*, 01969. [CrossRef]

39. Jeon, C. Adsorption of silver ions from industrial wastewater using waste coffee grounds. *Korean J. Chem. Eng.* **2017**, *34*, 384–391. [CrossRef]

40. Petala, A.; Bontemps, R.; Spartatouille, A.; Frontistis, Z.; Antonopoulou, M.; Konstantinou, I.; Kondarides, D.I.; Mantzavinos, D. Solar light-induced degradation of ethyl paraben with $CuO_x/BiVO_4$: Statistical evaluation of operating factors and transformation by-products. *Catal. Today* **2017**, *280*, 122–131. [CrossRef]

41. Frontistis, Z.; Antonopoulou, M.; Venieri, D.; Dailianis, S.; Konstantinou, I.; Mantzavinos, D. Solar photocatalytic decomposition of ethyl paraben in zinc oxide suspensions. *Catal. Today* **2017**, *280*, 139–148. [CrossRef]

42. Guo, J.; Shi, H.; Huang, X.; Shib, H.; An, Z. $AgCl/Ag_3PO_4$: A stable Ag-Based nanocomposite photocatalyst with enhanced photocatalytic activity for the degradation of parabens. *J. Colloid Interface Sci.* **2018**, *515*, 10–17. [CrossRef] [PubMed]

43. Chen, Y.; Deng, P.; Xie, P.; Shang, R.; Wang, Z.; Wang, S. Heat-activated persulfate oxidation of methyl- and ethyl-parabens: Effect, kinetics, and mechanism. *Chemosphere* **2017**, *168*, 1628–1636. [CrossRef] [PubMed]

44. Dhaka, S.; Kumar, R.; Lee, S.H.; Kurade, M.B.; Jeon, B.H. Degradation of ethyl paraben in aqueous medium using advanced oxidation processes: Efficiency evaluation of UV-C supported oxidants. *J. Clean. Prod.* **2018**, *180*, 505–513. [CrossRef]

45. Frontistis, Z.; Antonopoulou, M.; Yazirdagi, M.; Kilinc, Z.; Konstantinou, I.; Katsaounis, A.; Mantzavinos, D. Boron-doped diamond electrooxidation of ethyl paraben: The effect of electrolyte on by-products distribution and mechanisms. *J. Environ. Manag.* **2017**, *195*, 148–156. [CrossRef]